Germanium Anode with Excellent Lithium Storage Performance in a Germanium/Lithium–Cobalt Oxide Lithium-Ion Battery

Xiuwan Li,[†] Zhibo Yang,[†] Yujun Fu, Li Qiao, Dan Li, Hongwei Yue, and Deyan He*

School of Physical Science and Technology, Key Laboratory for Magnetism and Magnetic Materials of the Ministry of Education, Lanzhou University, Lanzhou 730000, China. [†]X.L. and Z.Y. contributed equally.

ABSTRACT Germanium is a highly promising anode material for lithium-ion batteries as a consequence of its large theoretical specific capacity, good electrical conductivity, and fast lithium ion diffusivity. In this work, Co_3O_4 nanowire array fabricated on nickel foam was designed as a nanostructured current collector for Ge anode. By limiting the voltage cutoff window in an appropriate range, the obtained Ge anode exhibits excellent lithium storage performance in half- and full-cells, which can be mainly attributed to the designed nanostructured current collector with good conductivity, enough buffering space for the volume change, and shortened ionic transport length. More importantly, the assembled Ge/$LiCoO_2$ full-cell shows a high energy density of 475 Wh/kg and a high power density of 6587 W/kg. A high capacity of 1184 mA h g^{-1} for Ge anode was maintained at a current density of 5000 mA g^{-1} after 150 cycles.

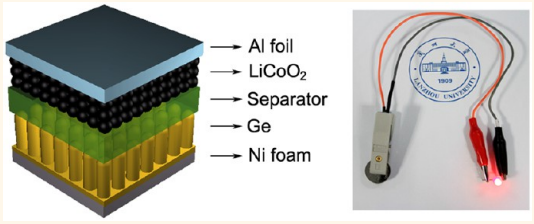

KEYWORDS: germanium coating · anode material · nanostructured current collector · full-cell · Co_3O_4 nanowires

Group IV elements (Si, Ge, Sn), which can alloy with lithium and result in relatively high theoretical specific capacities, are considered promising alternative anode materials to replace graphite for lithium-ion batteries (LIBs).[1−8] Compared with Si, Ge attracts less attention due to its higher cost and lower capacity.[9−11] However, the electrical conductivity of Ge is 10^4 higher than that of Si, and the diffusivity of Li ion in Ge is 400 times faster than that in Si at room temperature, which makes Ge be a more promising anode for high-power LIBs.[12−14] Unfortunately, similar to Si, the huge volume change (>300%) of Ge during the lithiation and delithiation processes hinders its practical application in LIBs.[15−17] Depositing Ge coating directly on a nanostructured current collector seems to be an efficient strategy to address the above issue because the nanostructured electrode can always accommodate the internal stress of the active material more efficiently.[18−24]

Wang *et al.* developed an architecture of depositing Ge film with a thickness of 1020 nm on a vertically aligned carbon nanotube (VACNT) array. Such a VACNT-supported thick Ge film electrode delivered a reversible capacity as high as 1314 mA h g^{-1}.[25] Liu *et al.* prepared a three-dimensional ordered macroporous Ge electrode directly onto copper foil *via* ionic liquid electrodeposition followed by a polystyrene template etching process, and the electrode exhibited a reversible capacity of 1024 mA h g^{-1} in the first cycle and a capacity of 844 mA h g^{-1} after 50 cycles.[26] Yu *et al.* coated 20-nm- and 50-nm-thick amorphous Ge thin films on 100-nm-thick three-dimensional bicontinuous Au electrodes, which delivered a high reversible capacity of 1066 mA h g^{-1} even after 100 cycles at 320 mA g^{-1}.[27] However, the fabrication of the nanostructured current collectors in the above-mentioned approaches cannot avoid complex procedures, rigorous experimental conditions, and sophisticated equipment, which greatly hinder these electrodes in the practical application of LIBs. It is essential to develop a facile way to prepare nanostructured current collectors.

* Address correspondence to hedy@lzu.edu.cn.

Received for review November 26, 2014 and accepted January 28, 2015.

Published online January 28, 2015
10.1021/nn506760p

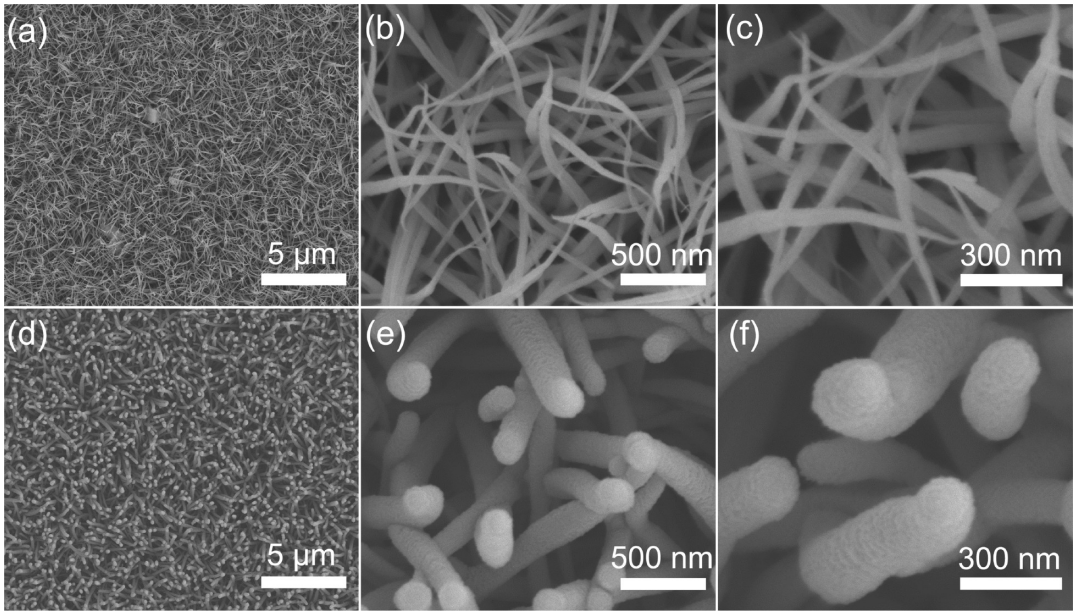

Figure 1. SEM images of (a–c) the synthesized Co_3O_4 nanowire array and (d–f) the resultant coaxial Ge/Co_3O_4 nanorod array.

In this work, we propose a strategy that uses a lithiated metal oxide as the electronic conductor of the current collector. Compared to the metal oxides, the Ge electrode has much lower (<0.5 V) discharge voltage plateaus. Therefore, setting an appropriate voltage cutoff window that only covers the discharge–charge voltage plateaus of Ge electrode can avoid the electrochemical reactions of the metal oxides. Among all the transition-metal oxides, cobalt oxide is considered as the most appropriate candidate due to its higher discharge–charge voltages (about 1.2 and 2.2 V). Meanwhile, a variety of nanostructured cobalt oxides can be directly fabricated on the metallic current collectors using some readily available ways.[28] To test the feasibility of this strategy, Ge/Co_3O_4 shell/core electrodes were prepared and assembled into half- and full-cells in the present work. Ge electrode with such a unique architecture exhibits high capacity, excellent rate capability, and cyclic stability in both the half- and full-cell configurations. The experimental results confirm that the lithiated Co_3O_4 nanowire array grown on Ni foam substrate is a perfect electronic conductor of the current collector for Ge anode.

RESULTS AND DISCUSSION

X-ray diffraction (XRD) patterns of the synthesized Co_3O_4 nanowire array and the resultant Ge/Co_3O_4nanostructrue on Ni foam are shown in Figure S1a (Supporting Information). The three strong diffraction peaks located at 44.4°, 51.7° and 76.2° come from the used Ni foam substrate, corresponding to the (111), (200), and (220) planes of cubic Ni, respectively (JCPDS 4-850). The other diffraction peaks for the sample of Co_3O_4 can be indexed to the (111), (220), (311), (422), (511), and (440) planes of spinel Co_3O_4, respectively (JCPDS 42-1467). All of the diffraction peaks were weakened after deposition of the Ge coating, and the fact that no additional peak can be observed indicates that the structure of the Ge coating is amorphous. Figure S1b (Supporting Information) shows Raman spectra of the samples. The peaks centered at 187, 466, 512, 609, and 674 cm^{-1} can be attributed to the F_{2g}, E_g, F_{2g}, F_{2g}, and A_{1g} vibration modes of spinel Co_3O_4 phase, respectively, which is consistent with the results of the XRD examination. After deposition of the Ge coating, two peaks centered at 270 and 170 cm^{-1} appeared, which can be interpreted as the signals from amorphous Ge coating.

Parts a–c of Figure 1 show scanning electron microscopy (SEM) images of the synthesized Co_3O_4 nanowire array. It can be seen that the Co_3O_4 nanowires were curved and intertwined with each other, forming a three-dimensional network structure. The average diameter of the as-prepared Co_3O_4 nanowires is around 50 nm. Parts d–f of Figure 1 present SEM images of the Ge-coated Co_3O_4 nanorod network. The synthesized Co_3O_4 nanowires were conformally coated with amorphous Ge, presenting a nanorod array structure in a panoramic view. The interconnected structure still remained after deposition of the Ge coating, which can be further confirmed in Figure S2 (Supporting Information). On the basis of Figure 1c,f, the thickness of the Ge coating was estimated to be about 60 nm. From the cross-sectional SEM image of the coaxial Ge/Co_3O_4 nanorods shown in Figure S2 (Supporting Information), it can be seen that not only the tip part but also the base part of the Co_3O_4 nanowires were coated with Ge, and the average height of the coaxial Ge/Co_3O_4 nanorods is about 5 μm.

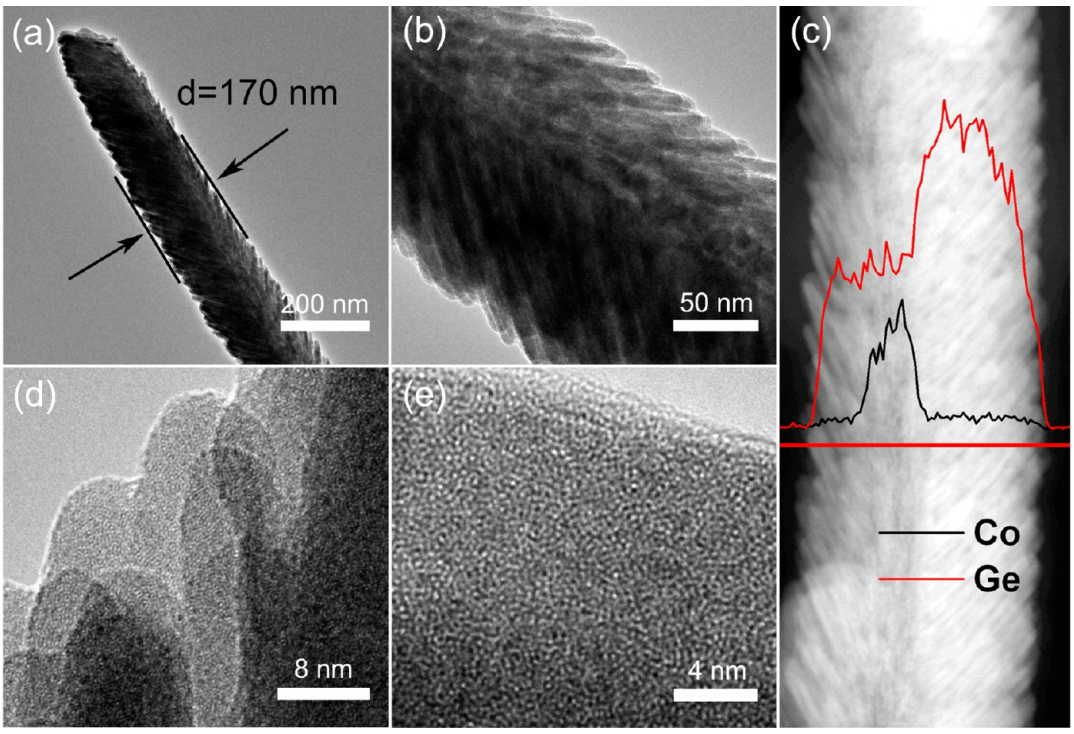

Figure 2. (a, b) TEM images of a single coaxial Ge/Co_3O_4 nanorod. (c) Cross-sectional STEM image of the Ge/Co_3O_4 nanorod. (d, e) The corresponding high-resolution TEM images of the Ge shell.

The morphology and structure of the Ge/Co_3O_4 nanorods were also characterized by transmission electron microscopy (TEM) as shown in Figure 2. Parts a and b of Figure 2 show that Ge was uniformly coated on the Co_3O_4 nanowires and exhibited a scalelike structure as the nanowires were almost directing at the source during the evaporation process. The elemental distribution across the nanorod was analyzed by energy-dispersive X-ray (EDX) spectroscopy mapping as shown in Figure 2c. It indicates that the outer coating is mainly composed of Ge, while Co only exists in the core of the nanorod, further confirming the core−shell structure of the nanorod (Figure S3, Supporting Information, for more details). From the high-magnification TEM images of the Ge shell shown in Figure 2d,e, it can be seen that the amorphous Ge coating is columnar growth which results in much free spaces between the small Ge columnars. Such a unique structure obviously benefits from the insertion/extraction of Li ions when the material is used as an anode for LIBs.

Figure 3a shows a schematic of the reactions for the Ge/Co_3O_4 nanorods with Li ions. The reaction voltages with Li ions are in the range of 1−3 V for Co_3O_4, while they are in the range under 1 V for Ge. Thus, as the voltage cutoff window of the cells is set from 0.02 to 1 V, there is only the reaction of Ge with Li ions within the Ge/Co_3O_4nanorods. More importantly, before the reaction of Ge shell with Li ions, the Co_3O_4 core can be first lithiated and become a composite of metallic Co and Li_2O. Because of the better conductivity of the metallic Co, the lithiated Co_3O_4 core is more suitable as an electronic conductor of the current collector in this situation.

To test the feasibility of the above idea, coin-type half-cells were assembled to investigate the electrochemical performance of the obtained Ge/Co_3O_4 nanorod array as an anode for LIBs. Figure S4 (Supporting Information) shows the cyclic voltammetric (CV) curves measured at a scan rate of 0.1 mV s^{-1} over a voltage range from 0.02 to 1 V. In the first cathodic scan, an intense peak positioned at 0.78 V can be observed, which should be associated with the initial reduction of Co_3O_4 ($Co_3O_4 + 8Li^+ + 8e^- \rightarrow 3Co + 4Li_2O$). It disappears in the subsequent cycles due to the test voltage limitation.[29] The peaks at about 0.40, 0.25, and 0.05 V can be ascribed to the formation of the Li_xGe alloys.[22−24] In the corresponding anodic scan, there is only one peak at about 0.59 V, which corresponds to the phase transition of Li_xGe to Ge. In the subsequent cycles, the three cathodic peaks shift to around 0.46, 0.32, and 0.15 V due to the drastic Li-driven structural or textural modifications during the first lithiation process.

Figure 3b shows that, for the electrode of the Ge/Co_3O_4 nanorod array tested in the voltage range from 1 to 0.02 V at a rate of 0.5 C (1 C was defined as 1000 mA g^{-1} to facilitate experimental parameter-setting), the initial discharge and charge capacities are 6088 and 1451 mA h g^{-1}, respectively. The abnormally high capacity for the first discharge can be mainly attributed to the lithiation of Co_3O_4, which is not involved in the active mass of the electrode. In the

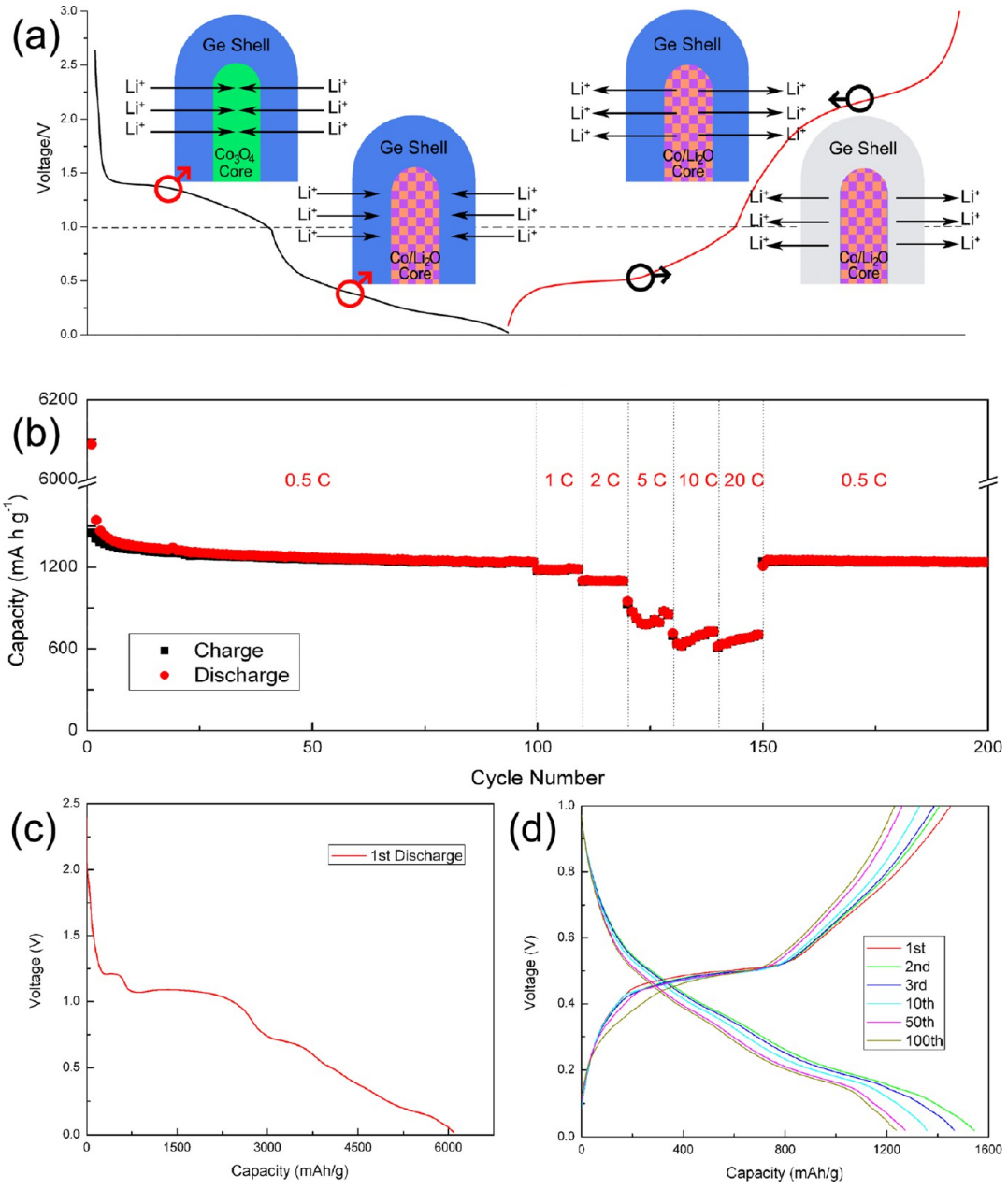

Figure 3. (a) Schematic of the reactions for the Ge/Co_3O_4 nanorods with Li-ions. (b) Galvanostatic discharge−charge cycling run at a rate of 0.5 C for 100 cycles and then at various rates from 1 to 20 C in a voltage range from 1 to 0.02 V. (c, d) Representative discharge−charge voltage profiles at the various cycles.

second cycle, the discharge capacity is 1543 mA h g^{-1}. The capacity shows a slight decrease and reaches 1237 mA h g^{-1} in the 100th cycle. After 100 cycles, the cell was diverted to the test of the rate performance. It can be seen that the capacities are relatively stable at the higher current densities, and the discharge capacities are 1181 (in the 105th cycle), 1099 (115th), 787 (125th), 686 (135th), and 675 mA h g^{-1} (145th) at rates of 1, 2, 5, 10, and 20 C, respectively. It is noted that the electrode recovers the capacity just before the rate test and reaches 1251 mA h g^{-1} in the 155th cycle when the current rate is returned to 0.5 C, indicating the excellent rate capability and the quite stable structure of the Ge/Co_3O_4 nanorod electrode. The representative discharge−charge voltage profiles at the corresponding C rates are shown in Figure S5 (Supporting Information).

Parts c and d of Figure 3 show the selected discharge−charge voltage profiles of the Ge/Co_3O_4 nanorod array electrode. The first discharge curve displays two well-defined voltage plateaus at about 1.20 and 1.05 V, corresponding to the reductions of Co^{3+} to Co^{2+} and Co^{2+} to Co, respectively.[29,31] Near 0.8 V there are some voltage plateaus corresponding to the alloying of Ge and Li. These results are consistent with the first anodic scan curve of the CV test shown in Figure S4

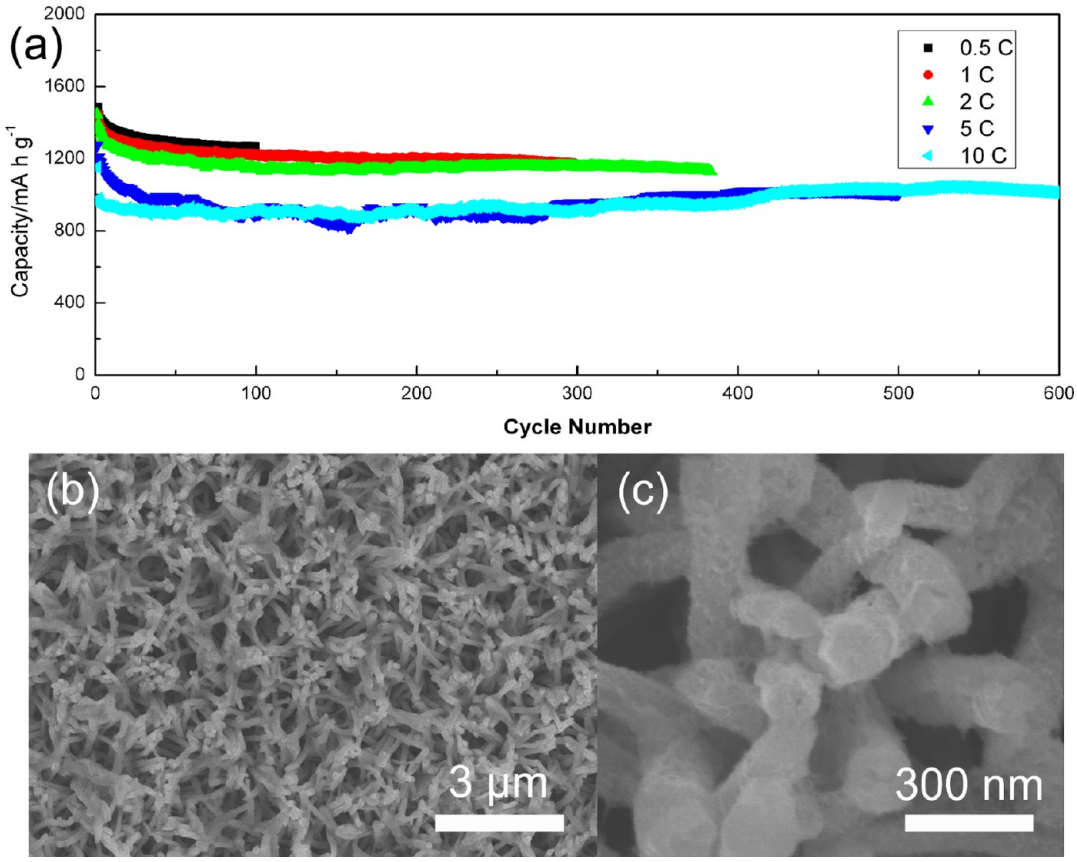

Figure 4. (a) Galvanostatic discharge−charge cycles at 0.5, 1, 2, 5, and 10 C. (b, c) SEM images of the coaxial Ge/Co_3O_4 nanorod array electrode after 100 cycles at 0.5 C.

(Supporting Information). Figure 3d shows the voltage profiles of the Ge/Co_3O_4 nanorod array electrode in the first (only charge curve), second, third, 10th, 50th, and 100th cycle measured in the range of 0.02−1.0 V at a rate of 0.5 C. It can be seen that, for all the discharge processes, there are three voltage plateaus at about 0.44, 0.36, and 0.17 V, which may be ascribed to the formation of the Li_xGe alloys. For all the charge processes, there is only one voltage plateau at 0.5 V. All the discharge−charge plateaus belong to the active Ge coating, indicating that the formed Co/Li_2O core does not partake in the electrochemical reactions under a limited voltage range of 0.02−1 V. To further prove this point, the capacity of the pure Co_3O_4 anode was tested within the voltage range of 0.02−1 V. It was found that the pure Co_3O_4 anode only has a capacity of 0.02 mA h, except the first discharge capacity of 0.67 mA h (Figure S6, Supporting Information).

More cells with the obtained Ge/Co_3O_4 nanorod array as an electrode were tested upon discharge−charge cycles at rates of 0.5, 1, 2, 5, and 10 C (Figure 4a). It can be seen that the electrodes show excellent capacity retention even at high rates. Especially at the highest rate of 10 C, the electrode can deliver a capacity as high as 1018 mA h g^{-1} after 600 cycles. The discharge capacities of the Ge/Co_3O_4 nanorod array electrodes at these rates are summarized in Table S1 (Supporting Information).

The top-view SEM images of the Ge/Co_3O_4 nanorod array electrode after 100 cycles at 0.5 C are shown in Figure 4b,c. The electrode seems to remain the nanorod array structure after cycles, which may be responsible for its excellent electrochemical stability. The superior electrochemical performance of the Ge/Co_3O_4 nanorod array anode can be explained as follows. First, the used Ni foam and the formed Co/Li_2O composite core can provide a good conductivity for Ge shell. Second, the structure of the nanorod array can supply enough space to buffer the volume change caused by the electrochemical reactions. Third, the nanostructure of the coaxial Ge/Co_3O_4 nanorods leads to shortened electronic and ionic transport lengths.

Furtherly we used the Ge/Co_3O_4 nanorod array as anode and the commercial $LiCoO_2$ (LCO) material as cathode to assemble a Ge/LCO full cell. More details about morphology, structure, and electrochemical property of the LCO cathode are shown in Figures S7 and S8 (Supporting Information). On the basis of the individual behaviors of the Ge/Co_3O_4 nanorod array and the LCO half-cells, it is possible that the Ge/LCO full-cell should have excellent electrochemical performance with high specific capacity and high-output working voltage.

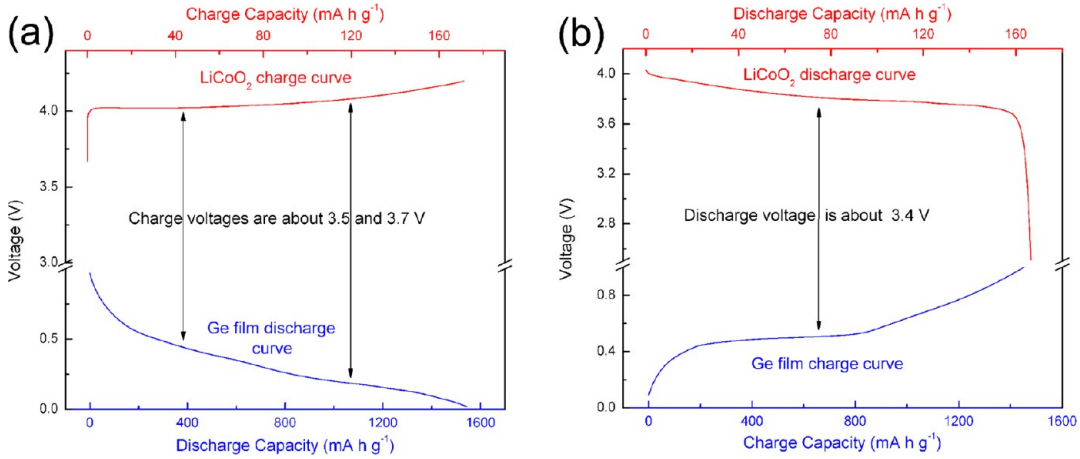

Figure 5. (a) Second charge (LCO electrode in half-cell, upper) and discharge (Ge electrode in half-cell, lower) curves. (b) Second discharge (LCO electrode in half-cell, upper) and charge (Ge electrode in half-cell, lower) curves.

Figure 5a shows the second discharge curve of the Ge/Co_3O_4 anode and the second charge curve of the LCO cathode in their respective half-cells. The discharge voltage plateaus of Ge anode are about 0.5 and 0.3 V, and the charge voltage plateau of LCO cathode is about 4.0 V. Thus, the charge voltage plateaus of the Ge/LCO full-cell should be about 3.5 and 3.7 V. As shown in Figure 5b, the discharge voltage plateau of the Ge/LCO full-cell is about 3.4 V. To set an appropriate voltage cutoff window, the discharge and charge curves of the Co_3O_4 anode and the LCO cathode were measured and shown in Figure S9 (Supporting Information). It can be clearly seen that the discharge and charge voltage plateaus of the Co_3O_4/LCO full-cell are about 1.7 and 2.6 V. Therefore, we designed the voltage cutoff window of the Ge/LCO full-cell as ~2.9−3.9 V for the small current densities.

To avoid the electrochemical reactions of the Co_3O_4 core during the first charge process in full-cell, Li-ions were first inserted by a chronopotentiometry using a special device as shown in Figure S10a (Supporting Information). Similar to the cell structure, there is electrolyte (as same as that in the cell) in a sealed bottle, and the Ge/Co_3O_4 nanorod array is the working electrode and lithium foil is the counter and reference electrode. As shown in Figure S10b (Supporting Information), setting the low cutoff voltage as 0.7 V can ensure that the Co_3O_4 nanowires were adequately lithiated even given the presence of the overpotential.

Figure 6a shows a schematic of the full-cell with Ge anode and LCO cathode. The capacity of the LCO cathode was designed as higher than that of the Ge/Co_3O_4 anode at a small current density. Figure 6b is a digital image of a light-emitting-diode (LED) lighting by the Ge/LCO full-cell.

CV curves of the Ge/LCO full-cell are shown in Figure 6c. In the first cycle, three peaks at 3.45, 3.60, and 3.80 V appear in anodic scan and only one strong peak at 3.36 V in cathodic scan. In the subsequent cycles, no potential shift can be found in these peaks. The CV curve shape of the Ge/LCO full-cell is consistent with that of the Ge anode half-cell, which indicates that the formed Co/Li_2O composite cores do not participate in the electrochemical reaction under a voltage cutoff window of 2.8−3.9 V.

Figure 6d reveals the corresponding cycling performance of the Ge/LCO full-cell at 0.5 C. Based on the active mass of the amorphous Ge coating, the initial discharge and charge capacities are 1969 and 1265 mA h g^{-1}, respectively. The higher initial capacity than the theoretical capacity and the irreversible capacity loss may be mainly attributed to the reduction of the Co_3O_4 nanowire cores, which only happens in the first charge process for the full-cell. The other irreversible processes such as the electrolyte decomposition and the inevitable formation of solid electrolyte interface (SEI) layer had happened before assembling the Ge anode into the full-cell.[30,31] In the subsequent cycles, the discharge capacity slowly reduces to 1100 mA h g^{-1} in the 100th cycle, whereas the Coulombic efficiency increases to 98.9%.

The high rate performance of the Ge/LCO full-cell was further evidenced by the capacity retention test at various C rates. As shown in Figure 6e, the cell was first charged/discharged at 0.5 C, and then the rate gradually increased to 20 C. The discharge specific capacities at 0.5, 1, 2, 5, and 10 C are 1319 (in the fifth cycle), 1244 (15th), 1295 (25th), 1278 (35th), and 1305 mA h g^{-1} (45th), respectively. Even at an extremely high rate of 20 C, it still releases a high discharge specific capacity of 1299 mA h g^{-1} (in the 55th cycle), which is 98.5% of the capacity at 0.5 C. Figure 6f shows the representative discharge/charge voltage profiles of the Ge/LCO full-cells at various C rates. Two main charge plateaus at ~3.6 and 3.8 V are observed (black line) in the fifth charge process at 0.5 C, while only one discharge plateau at about 3.4 V is noticed in

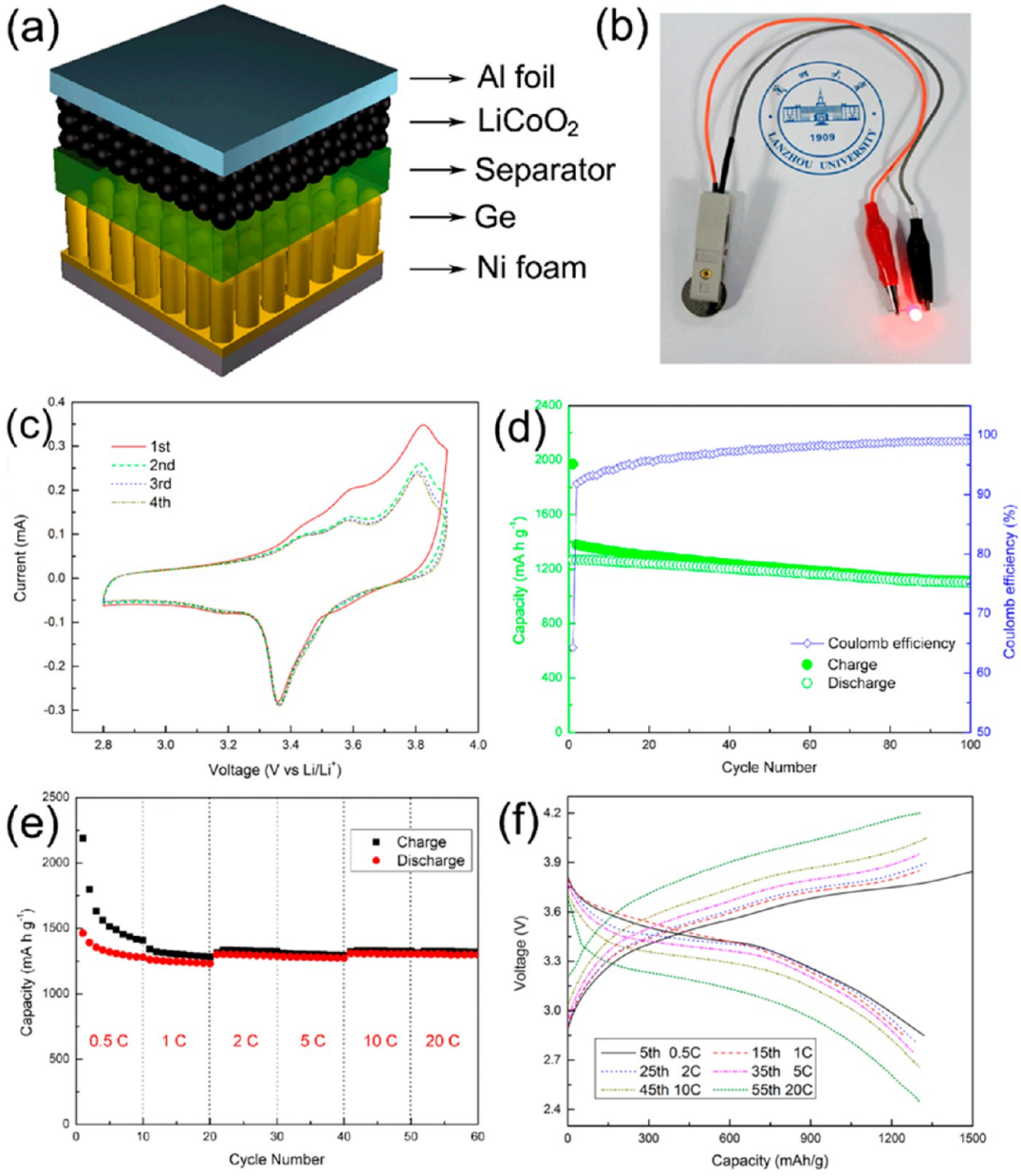

Figure 6. (a) Schematic of the Ge/LCO full-cell. (b) Digital image of a light-emitting diode lighted by the Ge/LCO full-cell. (c) Cyclic voltammograms of the initial four cycles for the Ge/LCO full-cell. (d) Charge−discharge cycling and Coulombic efficiency measured at a rate of 0.5 C for the Ge/LCO full-cell. (e) Capacity retention of the Ge/LCO full-cell at various *C* rates from 0.5 to 20 C. (f) Representative discharge−charge voltage profiles at various *C* rates for the Ge/LCO full-cell.

the corresponding discharge process. These are consistent with the discussion about the charge voltage plateau of the Ge/LCO full-cell. When the *C* rate is increased from 0.5 to 20 C, the discharge potential decreases and the charge potential increases. This phenomenon may be due to the kinetic effects of the material, rendering the higher overpotential. This high rate performance of the Ge/LCO full-cell can be attributed to the different settings of the voltage cutoff window for the full cell. With the higher overpotential caused by higher current density, the voltage cutoff window becomes wider, which makes all the voltage plateaus be contained in this voltage cutoff window. It is worth mentioning that, even at the highest rate of 20 C, the discharge voltage plateau can still be maintained at 3.1 V. It can be clearly seen that there are not charge/discharge plateaus of the Co_3O_4 nanowire cores, indicating that the strategy of limiting the voltage cutoff window to avoid the electrochemical reactions of the metal oxide is feasible.

To evaluate electrochemical performance of the Ge anode in the Ge/LCO full-cells, Ragone plot based on the masses of the active Ge and LCO materials is shown in Figure S11 (Supporting Information). The more detail about the calculation of energy and power can be

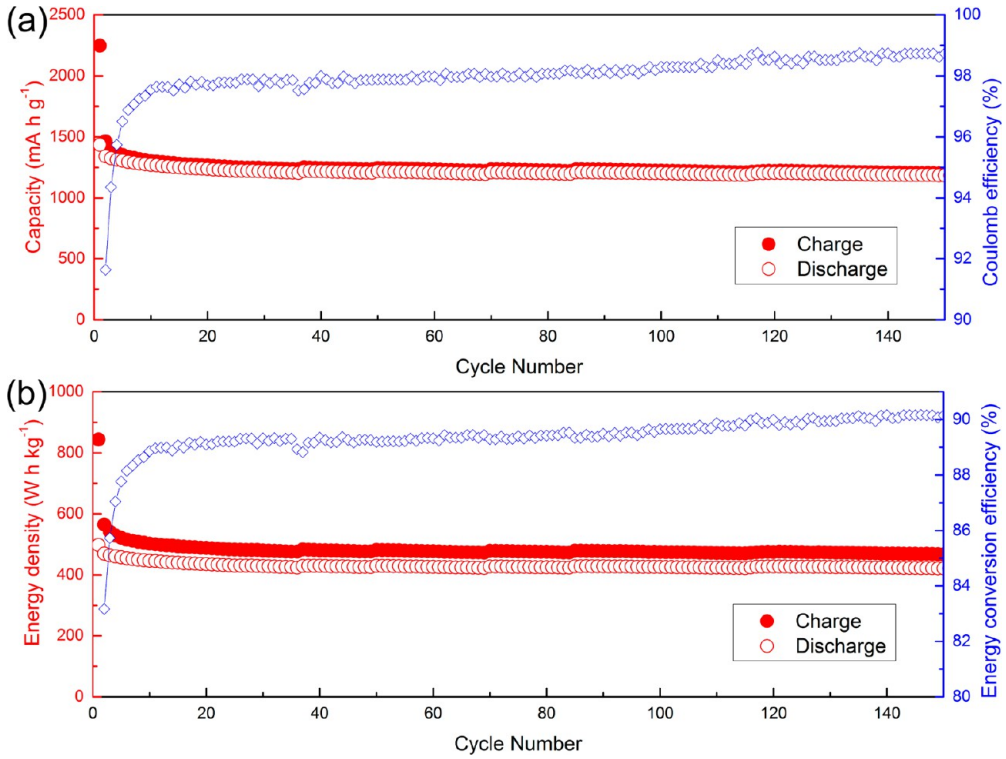

Figure 7. (a) Charge–discharge cycling and Coulombic efficiency for the Ge/LCO full-cell measured at a rate of 5 C. (b) Corresponding cycling performance of the energy density and the energy conversion efficiency.

found in the Supporting Information. Remarkably, the highest power density of 6623 W/kg and the maximum energy density of 504 Wh/kg were attained. More importantly, with an increase of the power density from 191.6 to 6623 W/kg, the energy density has a slight attenuation. Cyclic performance of a typical Ge/LCO full-cell at a rate of 5 C is shown in Figure 7a. The initial charge and discharge capacities calculated based on the mass of the amorphous Ge coating are 2246 and 1434 mA h g^{-1}, respectively. The irreversible capacity loss can be mainly attributed to the reduction of the Co_3O_4 nanowire cores. After 160 cycles, the discharge capacity can remain at 1184 mA h g^{-1}, and the Coulombic efficiency after the initial 10 cycles remains higher than 97.5%, indicating excellent electrochemical stability of the Ge anode in the full-cell. Figure 7b reveals the corresponding cycling performance of the energy density as well as its energy conversion efficiency. On the basis of the masses of the Ge anode and LCO cathode, the initial charge and discharge specific energies are 843 and 497 Wh/kg, respectively, giving an initial energy conversion efficiency of 59.0%. Similarly, a rather low initial energy conversion efficiency can be attributed to the reduction of the Co_3O_4 nanowire cores. In the subsequent cycles, the energy conversion efficiency slowly increases and steadily maintains at values higher than 89.1% after 20 cycles. In the 160th cycle, the discharge energy density is 421 Wh/kg, and the energy conversion efficiency reaches up to 90.2%. The high energy conversion efficiency can be attributed to the low voltage hysteresis of the Ge material, indicating that the Ge/Co_3O_4 nanorod array is a promising anode for LIBs. Overall, compared with the other full-cells such as Ge/$LiFePO_4$, $Li_4Ti_5O_{12}$/$LiFePO_4$, MnO/$LiNi_{0.5}Mn_{1.5}O_{4-\delta}$, Fe_2O_3/$LiFePO_4$, and Mn_2O_3/$LiMn_2O_4$, the present Ge/LCO full-cell has advantages including high specific capacity, high output working voltage, high energy and power density, and low energy conversion loss.[21,32–35]

CONCLUSION

In summary, Co_3O_4 nanowire array fabricated on nickel foam was designed as a nanostructured current collector for Ge anode of LIBs. By limiting the voltage cutoff window in an appropriate range, the obtained Ge anode exhibited excellent lithium storage performance. In the half-cells, it can deliver a high reversible capacity up to 1237 mA h g^{-1} after 100 cycles at 0.5 C and a capacity up to 1018 mA h g^{-1} in the 600th cycle at 10 C. The results indicated that the lithiated Co_3O_4 nanowire array after the first discharge is a promising electronic conductor of the nanostructured current collector for LIBs, which can buffer the volume change of the active material and shorten the diffusion length of lithium ions during the discharge/charge processes. More importantly, the assembled Ge/LCO full-cell showed a high energy density of 504 Wh/kg and a high power density of 6623 W/kg, and after 150 cycles, it still maintained a high capacity

of 1184 mA h g^{-1} at a rate of 5 C. The excellent lithium storage performance of the Ge/LCO full-cells indicated that the strategy of limiting the voltage cutoff window in an appropriate range to avoid the electrochemical reactions of the Co_3O_4 nanowires is feasible.

MATERIALS AND METHODS

Growth of the Co_3O_4 Nanowire Array on Ni Foam. $Co(NO_3)_2 \cdot 6H_2O$ (1 mmol) and $CO(NH_2)_2$ (10 mmol) were dissolved into 40 mL of deionized water, and the obtained solution and a piece of cleaned Ni foam were then transferred into a Teflon-lined stainless steel autoclave with a volume of 50 mL. The autoclave was heated at 90 °C for 6 h in an oven and cooled to room temperature naturally. The product was then annealed at 350 °C for 1 h in air.[29]

Deposition of the Ge Coating on the Co_3O_4 Nanowires. Amorphous Ge was coated onto the synthesized Co_3O_4 nanowire array by using an electron-beam evaporator. The purity of Ge is 99.9999%. The evaporation was conducted with a deposition rate of 0.2 nm s^{-1} under a high vacuum of 10^{-4} Pa. The thickness of the coating was monitored with a quartz thickness sensor. The Co_3O_4 nanowires/Ni foam was kept at 90 °C and steadily rotated over the evaporation source for obtaining a good thickness uniformity of the Ge coating. The mean mass loading of the Ge coating is 0.19 mg cm^{-2}.

Structural Characterization. The crystal structure of the resultant materials and the used Ni foam was characterized by X-ray powder diffraction (Rigaku D/Max-2400 with Cu Kα radiation, $\lambda = 0.15418$ nm) with 2θ range from 10° to 90° and micro-Raman spectrometer (Jobin-Yvon LabRAM HR800 UV) with a radiation of 532 nm. The morphology of the samples was observed using field-emission scanning electron microscopy (S-4800, Hitachi) and transmission electron microscopy (FEI, Tecnai G2 F30).

Electrochemical Characterization. For electrochemical characterization, CR-2032 coin cells were assembled in a high-purity argon-filled glovebox (H_2O, O_2 < 0.5 ppm, MBraun, Unilab). The prepared Ge/Co_3O_4 nanorod array and/or the casted LCO material were the working electrodes, and lithium foil was the counter and reference electrode. Celgard 2320 was used as the separator membrane. The electrolyte was 1 M $LiPF_6$ dissolved in a mixture of ethylene carbonate (EC) and diethyl carbonate (DEC) in a 1:1 volume ratio. The LCO electrodes were prepared by spreading a mixture of 80 wt % LCO powder, 10 wt % acetylene black, and 10 wt % poly(vinylidene fluoride) on to an aluminum foil current collector. The as-casted electrodes were dried at 80 °C for 12 h and then 120 °C for 4 h in a vacuum oven.

The galvanostatic charge−discharge cycling, cyclic voltammetry, and electrochemical impedance spectrum measurements were carried out at room temperature by using a multichannel battery tester (Neware BTS-610) and an electrochemical workstation (CHI 660C). The voltage cutoff window was 0.02−1 V for the half-cells, while it was 2.8−3.8 V for the full-cells.

Conflict of Interest: The authors declare no competing financial interest.

Supporting Information Available: Additional Figures S1−S11, Table S1, their captions, and supplementary discussions. This material is available free of charge *via* the Internet at http://pubs.acs.org.

Acknowledgment. This work was financially supported by the National Natural Science Foundation of China (Grant Nos. 11179038 and 10974073) and the Specialized Research Fund for the Doctoral Program of Higher Education (Grant No. 20120211130005). Y.F. gratefully acknowledges the support of the Fundamental Research Funds for the Central Universities (Grant No. lzujbky-2014-35).

REFERENCES AND NOTES

1. Wang, D.; Yang, Z.; Li, F.; He, D. The Microstructure and Optical Properties of Crystallized Hydrogenated Silicon Films Prepared by Very High Frequency Glow Discharge. *Appl. Surf. Sci.* **2011**, *257*, 8350–8354.
2. Derrien, G.; Hassoun, J.; Panero, S.; Scrosati, B. Nanostructured Sn−C Composite as an Advanced Anode Material in High-Performance Lithium-Ion Batteries. *Adv. Mater.* **2007**, *19*, 2336–2340.
3. Ge, M.; Rong, J.; Fang, X.; Zhou, C. Porous Doped Silicon Nanowires for Lithium Ion Battery Anode with Long Cycle Life. *Nano Lett.* **2012**, *12*, 2318–2323.
4. Song, T.; Cheng, H.; Choi, H.; Lee, J.-H.; Han, H.; Lee, D. H.; Yoo, D. S.; Kwon, M.-S.; Choi, J.-M.; Doo, S. G.; et al. Si/Ge Double-Layered Nanotube Array as a Lithium Ion Battery Anode. *ACS Nano* **2011**, *6*, 303–309.
5. Wang, J.; Du, N.; Song, Z.; Wu, H.; Zhang, H.; Yang, D. Synthesis of Nanoporous Three-Dimensional Current Collector for High-Performance Lithium-Ion Batteries. *RSC Adv.* **2013**, *3*, 7543–7548.
6. Lou, X. W.; Deng, D.; Lee, J. Y.; Feng, J.; Archer, L. A. Self-Supported Formation of Needlelike Co3O4 Nanotubes and Their Application as Lithium-Ion Battery Electrodes. *Adv. Mater.* **2008**, *20*, 258–262.
7. Mahenderkar, N. K.; Liu, Y.-C.; Koza, J. A.; Switzer, J. A. Electrodeposited Germanium Nanowires. *ACS Nano* **2014**, *8*, 9524–9530.
8. McDowell, M. T.; Lee, S. W.; Nix, W. D.; Cui, Y. 25th Anniversary Article: Understanding the Lithiation of Silicon and Other Alloying Anodes for Lithium-Ion Batteries. *Adv. Mater.* **2013**, *25*, 4966–4985.
9. Su, X.; Wu, Q.; Li, J.; Xiao, X.; Lott, A.; Lu, W.; Sheldon, B. W.; Wu, J. Silicon-Based Nanomaterials for Lithium-Ion Batteries: A Review. *Adv. Energy Mater.* **2014**, *4*, 1300882–1300882.
10. Liu, Y.; Zhang, S.; Zhu, T. Inside Cover: Germanium-Based Electrode Materials for Lithium-Ion Batteries (ChemElectroChem 4/2014). *ChemElectroChem* **2014**, *1*, 817–817.
11. Yu, Y.; Yan, C.; Gu, L.; Lang, X.; Tang, K.; Zhang, L.; Hou, Y.; Wang, Z.; Chen, M. W.; Schmidt, O. G.; et al. Three-Dimensional (3D) Bicontinuous Au/Amorphous-Ge Thin Films as Fast and High-Capacity Anodes for Lithium-Ion Batteries. *Adv. Energy Mater.* **2013**, *3*, 281–285.
12. Tan, L. P.; Lu, Z.; Tan, H. T.; Zhu, J.; Rui, X.; Yan, Q.; Hng, H. H. Germanium Nanowires-Based Carbon Composite as Anodes for Lithium-Ion Batteries. *J. Power Sources* **2012**, *206*, 253–258.
13. Fuller, C. S.; Severiens, J. C. Mobility of Impurity Ions in Germanium and Silicon. *Phys. Rev.* **1954**, *96*, 21–24.
14. Liu, J.; Song, K.; Zhu, C.; Chen, C.-C.; van Aken, P. A.; Maier, J.; Yu, Y. Ge/C Nanowires as High-Capacity and Long-Life Anode Materials for Li-Ion Batteries. *ACS Nano* **2014**, *8*, 7051–7059.
15. Kennedy, T.; Mullane, E.; Geaney, H.; Osiak, M.; O'Dwyer, C.; Ryan, K. M. High-Performance Germanium Nanowire-Based Lithium-Ion Battery Anodes Extending over 1000 Cycles Through *in situ* Formation of a Continuous Porous Network. *Nano Lett.* **2014**, *14*, 716–723.
16. Seng, K. H.; Park, M.-H.; Guo, Z. P.; Liu, H. K.; Cho, J. Self-Assembled Germanium/Carbon Nanostructures as High-Power Anode Material for the Lithium-Ion Battery. *Angew. Chem., Int. Ed.* **2012**, *51*, 5657–5661.
17. Yan, C.; Xi, W.; Si, W.; Deng, J.; Schmidt, O. G. Highly Conductive and Strain-Released Hybrid Multilayer Ge/Ti Nanomembranes with Enhanced Lithium-Ion-Storage Capability. *Adv. Mater.* **2013**, *25*, 539–544.
18. Wang, D.; Yang, Z.; Li, F.; Liu, D.; Wang, X.; Yan, H.; He, D. Improved Performance For Lithium-Ion Batteries with

Nickel Nanocone-Arrays Supported Germanium Anode. *Mater. Lett.* **2011**, *65*, 1542–1544.
19. Rudawski, N. G.; Darby, B. L.; Yates, B. R.; Jones, K. S.; Elliman, R. G.; Volinsky, A. A. Nanostructured Ion Beam-Modified Ge Films for High Capacity Li Ion Battery Anodes. *Appl. Phys. Lett.* **2012**, *100*, 083111–083111.
20. Wang, C. D.; Chui, Y. S.; Li, Y.; Chen, X. F.; Zhang, W. J. Binder-free Ge-Three Dimensional Graphene Electrodes for High-Rate Capacity Li-Ion Batteries. *Appl. Phys. Lett.* **2013**, *103*, 253903–253903.
21. DiLeo, R. A.; Frisco, S.; Ganter, M. J.; Rogers, R. E.; Raffaelle, R. P.; Landi, B. J. Hybrid Germanium Nanoparticle−Single-Wall Carbon Nanotube Free-Standing Anodes for Lithium Ion Batteries. *J. Phys. Chem. C* **2011**, *115*, 22609–22614.
22. Zhang, C.; Pang, S.; Kong, Q.; Liu, Z.; Hu, H.; Jiang, W.; Han, P.; Wang, D.; Cui, G. An Elastic Germanium-Carbon Nanotubes-Copper Foam Monolith as an Anode for Rechargeable Lithium Batteries. *Rsc Adv.* **2013**, *3*, 1336–1340.
23. Yuan, F.-W.; Tuan, H.-Y. Scalable Solution-Grown High-Germanium-Nanoparticle-Loading Graphene Nanocomposites as High-Performance Lithium-Ion Battery Electrodes: An Example of a Graphene-Based Platform toward Practical Full-Cell Applications. *Chem. Mater.* **2014**, *26*, 2172–2179.
24. Park, M.-H.; Kim, K.; Kim, J.; Cho, J. Flexible Dimensional Control of High-Capacity Li-Ion-Battery Anodes: From 0D Hollow to 3D Porous Germanium Nanoparticle Assemblies. *Adv. Mater.* **2010**, *22*, 415–418.
25. Wang, X.; Susantyoko, R. A.; Fan, Y.; Sun, L.; Xiao, Q.; Zhang, Q. Vertically Aligned CNT-Supported Thick Ge Films as High-Performance 3D Anodes for Lithium Ion Batteries. *Small* **2014**, *10*, 2826–2829.
26. Liu, X.; Zhao, J.; Hao, J.; Su, B.-L.; Li, Y. 3D Ordered Macroporous Germanium Fabricated by Electrodeposition from an Ionic Liquid and Its Lithium Storage Properties. *J. Mater. Chem. A* **2013**, *1*, 15076–15081.
27. Yu, Y.; Yan, C. L.; Gu, L.; Lang, X. Y.; Tang, K.; Zhang, L.; Hou, Y.; Wang, Z. F.; Chen, M. W.; Schmidt, O. G.; et al. Three-Dimensional (3D) Bicontinuous Au/Amorphous-Ge Thin Films as Fast and High-Capacity Anodes for Lithium-Ion Batteries. *Adv. Energy Mater.* **2013**, *3*, 281–285.
28. Wang, X.; Fan, Y.; Susantyoko, R. A.; Xiao, Q.; Sun, L.; He, D.; Zhang, Q. High Areal Capacity Li Ion Battery Anode Based on Thick Mesoporous Co_3O_4 Nanosheet Networks. *Nano Energy* **2014**, *5*, 91–96.
29. Fu, Y.; Li, X.; Sun, X.; Wang, X.; Liu, D.; He, D. Self-Supporting Co_3O_4 with Lemongrass-Like Morphology as a High-Performance Anode Material for Lithium Ion Batteries. *J. Mater. Chem.* **2012**, *22*, 17429–17431.
30. Wang, C.; Wang, D. L.; Wang, Q. M.; Chen, H. J. Fabrication and Lithium Storage Performance of Three-Dimensional Porous NiO as Anode for Lithium-Ion Battery. *J. Power Sources* **2010**, *195*, 7432–7437.
31. Poizot, P.; Laruelle, S.; Grugeon, S.; Dupont, L.; Tarascon, J. M. Searching for New Anode Materials for the Li-Ion Technology: Time to Deviate from the Usual Path. *J. Power Sources* **2001**, *97−8*, 235–239.
32. Li, N.; Chen, Z. P.; Ren, W. C.; Li, F.; Cheng, H. M. Flexible Graphene-Based Lithium Ion Batteries with Ultrafast Charge and Discharge Rates. *Proc. Natl. Acad. Sci. U.S.A.* **2012**, *109*, 17360–17365.
33. Xu, G.-L.; Xu, Y.-F.; Fang, J.-C.; Fu, F.; Sun, H.; Huang, L.; Yang, S.; Sun, S.-G. Facile Synthesis of Hierarchical Micro/Nanostructured MnO Material and Its Excellent Lithium Storage Property and High Performance as Anode in a MnO/$LiNi_{0.5}Mn_{1.5}O_{4-\delta}$ Lithium Ion Battery. *ACS Appl. Mater. Interfaces* **2013**, *5*, 6316–6323.
34. Hassoun, J.; Croce, F.; Hong, I.; Scrosati, B. Lithium-Iron Battery: Fe_2O_3 Anode *versus* $LiFePO_4$ Cathode. *Electrochem. Commun.* **2011**, *13*, 228–231.
35. Wang, Y.; Wang, Y.; Jia, D.; Peng, Z.; Xia, Y.; Zheng, G. All-Nanowire Based Li-Ion Full Cells Using Homologous Mn_2O_3 and $LiMn_2O_4$. *Nano Lett.* **2014**, *14*, 1080–1084.